Nanoscale

ROYAL SOCIETY OF CHEMISTRY

COMMUNICATION

View Article Online
View Journal | View Issue

Check for updates

Cite this: *Nanoscale*, 2021, **13**, 9177

Received 22nd March 2021,
Accepted 14th April 2021

DOI: 10.1039/d1nr01805a

rsc.li/nanoscale

A novel visible light sensing and recording system enabled by integration of photodetector and electrochromic devices†

Wenqiang Wu,‡[a,b] Mengmeng Zhou,‡[c] Dong Li,‡[a] Shengman Li,[a] Zheng Yang,[b] Zhihao Huo,[b] Yanqing Wu,[d] Yongwen Tan,[a] Xun Han,*[e] Caofeng Pan*[b] and Anlian Pan*[a]

The integration of multiple electronic or optoelectronic devices is an effective strategy to use their unique functions to realize a specific goal. A state-of-the-art photodetector (PD) array can realize real-time image sensing, but the image information will disappear immediately with the removal of the light stimuli. Here, we design a visible light sensing and recording system by the integration of a perovskite PD array with a tungsten trioxide-based electrochromic device (ECD) array (10 × 10 pixels). The system can convert the received visible light signals into electrical signals to change the storable color of the corresponding pixels in the ECD array, thus realizing optical information recording in the form of the color display. As a conceptual demonstration, the system achieves the recording of the "H"-shaped visible light pattern projected to the active area of the PD array. Besides, after removing the illumination stimuli, the recording of the light pattern continues in the absence of the power supply owing to the "color memory effect". The recorded length can be regulated through the periods of illumination stimulation. The proof-of-concept system may have potential applications in image sensors, electronic eyes, and intelligent electronics.

Introduction

Photodetectors (PDs), as a vital component that converts optical signals into electrical signals, have attracted wide attention for light communication, image sensing, environmental monitoring, and other related fields.[1–6] Recently, various high performance PDs have been fabricated based on emerging optoelectronic semiconductor materials, such as two-dimensional materials and perovskite materials.[7–12] In particular, the perovskite materials have become one of the ideal materials due to their outstanding photoelectric properties, including large absorption coefficient, high carrier diffusion length and lifetime, tunable bandgaps, and low defect density.[13–17] The perovskite-based PDs have achieved significant breakthroughs in detectivity, response time, flexibility, and array integration.[18–24] For example, the detectivity of perovskite-based PDs reported by Feng *et al.* has exceeded 7×10^{15} Jones.[25] Besides, Gu and their colleagues integrated a large-scale PD array (1024 pixels) based on vertical $CH_3NH_3PbI_3$ perovskite nanowires.[26] However, the state-of-the-art PDs could only detect optical signals, which lack the capability of further processing signals. The recording of optical information always depends on other auxiliary instruments. Thus, an integrated optical information sensing and recording system should be explored.

Electrochromic devices (ECD) with a simple two-terminal device structure design can convert electrical signals into color variations.[27–31] Besides, they have the unique property of color retention without a power supply, which is called the "color memory effect".[32–34] The memory time can be regulated through the applied voltage as well as the voltage duration. These advantages make them a promising candidate for optical information recording. Therefore, by integrating a PD array with an ECD array, the received light signals can be directly expressed by color changes in the ECD array, realizing optical information sensing and recording.

Here, we designed a visible light sensing and recording system that consists of a perovskite PD array and a tungsten tri-

[a]*Key Laboratory for Micro-Nano Physics and Technology of Hunan Province, State Key Laboratory of Chemo/Biosensing and Chemometrics, and College of Materials Science and Engineering, Hunan University, Changsha, Hunan 410082, China. E-mail: anlian.pan@hnu.edu.cn*
[b]*CAS Center for Excellence in Nanoscience, Beijing Key Laboratory of Micro-nano Energy and Sensor, Beijing Institute of Nanoenergy and Nanosystems, Chinese Academy of Sciences, Beijing 100083, P. R. China. E-mail: cfpan@binn.cas.cn*
[c]*ARC Research Hub for Computational Particle Technology, Department of Chemical Engineering, Monash University, Clayton, Victoria 3800, Australia*
[d]*Institute of Microelectronics and Key Laboratory of Microelectronic Devices and Circuits (MOE) and Frontiers Science Center for Nano-optoelectronics, Peking University, Beijing, 100871, China*
[e]*College of Mechatronics and Control Engineering, Shenzhen University, Shenzhen, 518060, China. E-mail: hanxun@szu.edu.cn*
†Electronic supplementary information (ESI) available. See DOI: 10.1039/d1nr01805a
‡These authors contributed equally to this study.

oxide (WO_3)-based ECD array (10 × 10 pixels). The visible light signals were captured through the PD array and then converted into electrical signals to change the storable color of the corresponding pixels in the ECD array, thus realizing optical information sensing and recording in the form of a color display. As a conceptual demonstration, the system achieved the recording of the "H"-shaped visible light pattern projected to the active area of the PD array. Besides, after removing the illumination stimuli, the recording of the light pattern continued in the absence of thepower supply and the recorded length can be increased by extending the light stimulation time. When the duration of the illumination stimulus was 100 s, the recorded light pattern could still be recognized with little attenuation after 4 hours. Such a system may have potential applications in image sensors, electronic eyes, and intelligent electronics.

Results and discussion

Fig. 1a demonstrates the schematic illustration of the visible light sensing and recording system, where the perovskite PD array is functionalized to convert external optical stimuli to electrical signals and the WO_3-based ECD array is employed to record the optical information. Structurally, one end of the interdigital electrodes of the PD is connected to the bottom electrode of the ECD device, forming the integrated PD–ECD array in series. The detailed fabrication processes of the system could be found in the Experimental section and Fig. S1 (ESI).† Fig. 1b shows the simplified equivalent circuit diagram of a single unit of the system. The resistance of the pixels of the PD array can be switched from a high resistance state (HRS) to a low resistance state (LRS) by light triggering and the color of the ECD device can be tuned by the applied voltage. Under the dark conditions, the PD pixel possessing the HRS will occupy a large voltage in the series voltage, thus the partial voltage of the ECD device is too small to change the color state. With an increase in the intensity of light stimuli, the resistance state of the PD pixel will change from the HRS to LRS gradually, leading to an increase in the partial voltage of the ECD pixel. Subsequently, the coloration process occurs while the partial voltage is over the threshold. After removing the light stimuli, the "color memory effect" of the ECD will retain the color display for some time even if there is no power supply. Therefore, the optical information can be recorded in the form of the color display.

The PD array consists of 10 × 10 addressable pixels, in which each pixel acts as an independent photoreceptor cell. As schematically illustrated in Fig. 2a, the configuration of the individual pixel is a two-terminal photoconductive-type PD. All pixels share a drain electrode, and the other end is connected to the corresponding pixel in the ECD array (Fig. S2, ESI†). As previously reported, the organic–inorganic hybrid perovskite materials possess outstanding optoelectronic properties.[35–39] Here, the organic–inorganic hybrid $CH_3NH_3PbI_{3-x}Cl_x$ perovskite films were employed as the photosensitive material. For constructing individually addressable pixels, the perovskite films were controllably synthesized utilizing the previously reported two-step sequential deposition method.[40,41] Fig. 2b shows the scanning electron microscopy (SEM) image of the $CH_3NH_3PbI_{3-x}Cl_x$ perovskite film array, demonstrating the perovskite films with regular circular shape neatly arranged. It can be seen from the partially enlarged SEM image that the films have a compact surface with few pinhole defects (Fig. 2c). X-ray diffraction (XRD) of the as-synthesized perovskite films shows the strong characteristic peaks at 14.1° and 28.5° (Fig. S3, ESI†), which is consistent with the tetragonal structure of the previously reported $CH_3NH_3PbI_{3-x}Cl_x$ perovskite film.[42,43] As shown in Fig. 2d, the absorption range of the perovskite film spans the whole visible light region (380–790 nm), indicating that the material is suitable for fabricating visible light PDs.

To match with the coloring voltage of the ECD, the working current range of the PD can be tuned in the two-terminal planar configuration by regulating the active areas in each pixel. As demonstrated in Fig. S4 (ESI),† different amounts of perovskite films with dimensions of 200 × 200 μm^2 were grown on the interdigital electrode (1 × 1 mm^2). Five types of the PD with active areas of 0.04 cm^2, 0.08 cm^2, 0.16 cm^2, 0.36 cm^2, and 0.64 cm^2 were fabricated and the corresponding photoresponse behaviors were evaluated. Fig. 2e shows the current–voltage (I–V) curves at a bias voltage of 5 V, and the dark current was adjusted from 10^{-9} A to 10^{-7} A with the pixel area increasing from 0.04 cm^2 to 0.64 cm^2. Fig. 2f summarizes the

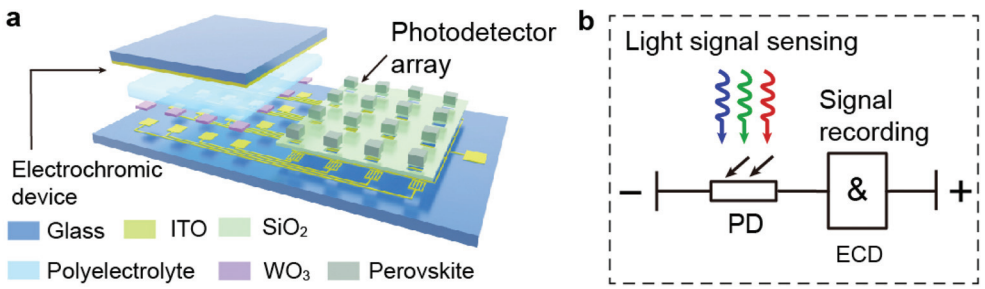

Fig. 1 Schematic illustration of the visible light sensing and recording system. (a) The structure of the visible light sensing and recording system. (b) The simplified equivalent circuit diagram of a single unit of the system.

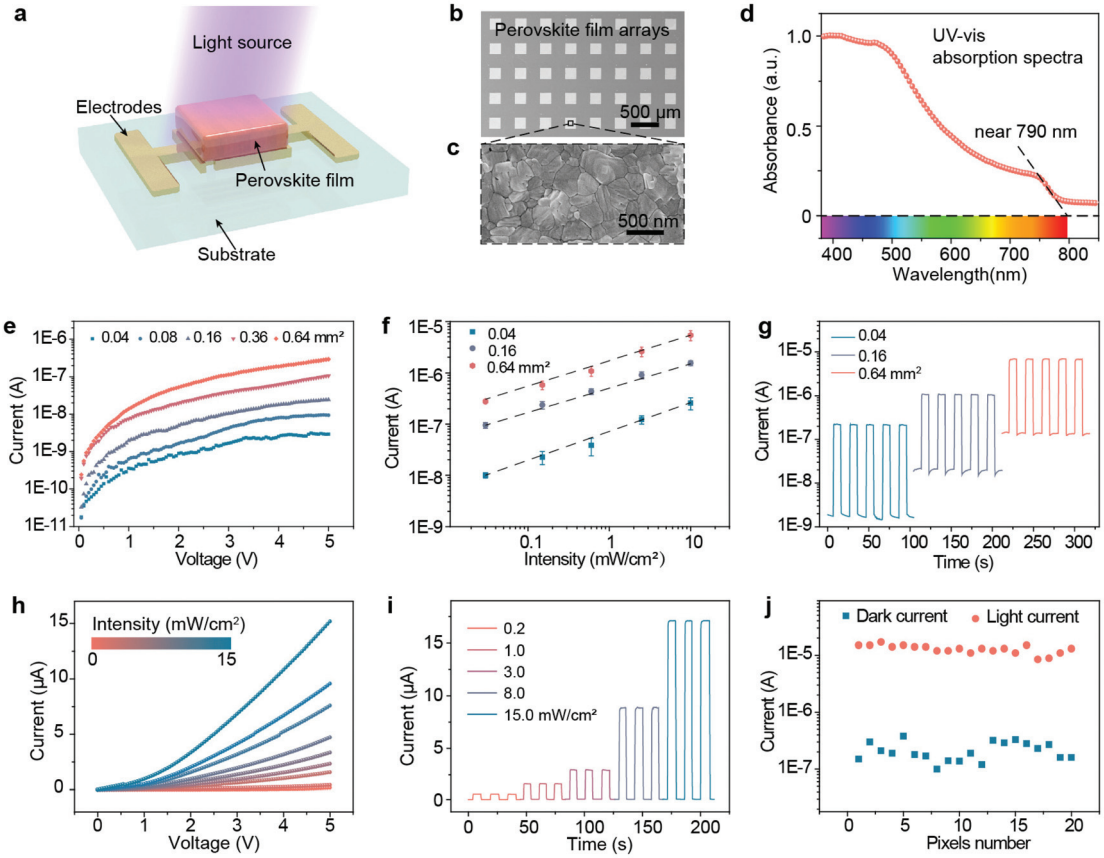

Fig. 2 Visible light sensing characteristics of the PD array. (a) Schematic illustration of an individual PD structure. (b and c) SEM images of the as-synthesized patterned perovskite films. (d) The absorption spectrum of the as-synthesized perovskite films. (e) The *I*–*V* curves of the single-pixel were adjusted by changing the perovskite film areas. (f and g) The dependence of photocurrent on the light intensity at +5 V bias voltage for pixels with different active areas and the corresponding dynamic response curves at a light intensity of 10 mW cm^{-2}. (h–j) The photoresponse of the PD with an active area of 0.64 mm^2. The *I*–*V* curves and *I*–*t* curves of the PD at different illumination intensities. The statistics of dark current and photocurrent (light intensity of 10 mW cm^{-2}) of 20 pixels in the PD array.

dependence of photocurrent on the light intensity at a +5 V bias voltage for pixels with different active areas. Under the same light stimuli, the photocurrent was enhanced with the pixel areas increasing from 0.04 cm^2 to 0.64 cm^2, which is due to the production of more photon-generated carriers in the larger active area. The corresponding dynamic response curves at a light intensity of 10 mW cm^{-2} are presented in Fig. 2g. It can be seen that the PDs with different active areas exhibit stable photoswitching characteristics with an on/off current ratio of about two orders of magnitude. The investigated results show the output current of the PD can be controlled by changing the dimension of perovskite films to match with the working voltage of the ECD.

The PD array with an active area of 0.64 cm^2 was employed to integrate with the ECD and its photoelectric properties were systematically characterized as shown in Fig. 2h–j. Current–voltage (*I*–*V*) curves of the PD were measured in the dark and under the illumination of white light. At a bias voltage of 5 V, the dark current was as low as about 1×10^{-7} A, while the photocurrent increased to 1.53×10^{-5} A at a light intensity of 15 mW cm^{-2}, exhibiting an on/off current ratio of two orders of magnitude (Fig. 2h). The dynamic response curves of the PD with the illumination intensity increasing from 0.2 mW cm^{-2} to 15 mW cm^{-2} are shown in Fig. 2i. As presented in Fig. S5a (ESI),† the current–time (*I*–*t*) of the PD remained nearly unchanged after operating for 150 cycles, illustrating the reversible and stable photoswitching characteristics. The rise time, defined from 10% to 90% of the saturated current value, and the decay time, defined from 90% to 10% of the saturated current value, were estimated as 25 ms and 30 ms, respectively (Fig. S5b, ESI†). Besides, the uniformity of the device was evaluated by the statistics of dark current and photocurrent of 20 pixels (two lines). As shown in Fig. 2j, both the photocurrent and the dark current were distributed within a narrow range, which illustrates that the device possesses a gratifying uniformity.

The layered-structure of the ECD is schematically presented in Fig. 3a and consists of a transparent substrate (glass), a transparent conductive layer (ITO), an ionic conductive layer (polyelectrolyte), electrochromic films, another transparent conductive layer (ITO), and a transparent glass. To facilitate the integration of the device, the polyelectrolyte prepared with

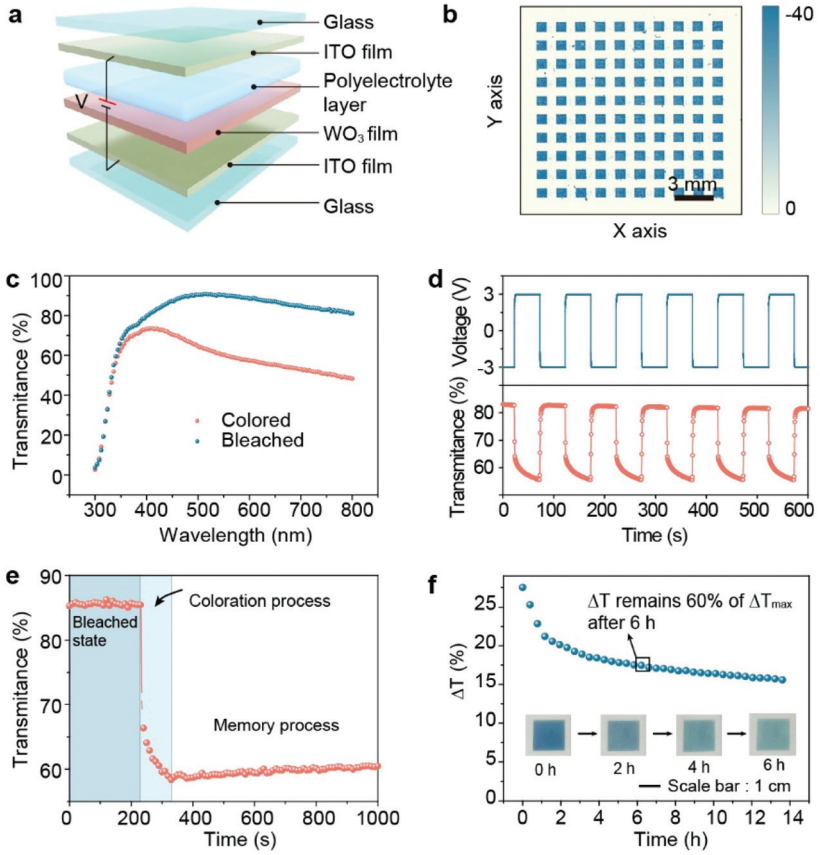

Fig. 3 The characterization of the ECD array. (a) Schematic illustration of the layered structure of the ECD. (b) The grayscale image of 100 pixels in the colored state. (c) The transmittance spectra from 300 to 800 nm of the device in the colored and bleached states. (d) The switching test between coloration and bleaching of the as-fabricated ECD at the wavelength of 633 nm. (e) The transmittance changes of the device in the coloration and memory process. (f) The ΔT changes of the device after the external electric field disappears. The inset photographs present a gradual fading process of the colored device over time.

anhydrous $LiClO_4$ and poly(methylmethacrylate) (PMMA) particles mixed in propylene carbonate was employed as the ionic conductive layer. The WO_3 film was selected as the electrochromic layer due to its high optical adjustment ability and outstanding electrochromic stability.[44–46] The principle of coloration and bleaching process is related to the intercalation/de-intercalation of electrons and small cations (such as H^+, Li^+, *etc.*), which can be explained by the following reversible reaction:[47]

$$WO_3 + xe^- + xLi^+ \rightleftharpoons Li_xWO_3 \quad (1)$$

Under the positive electric field stimulus, Li^+ ions and e^- are inserted into the WO_3 films to form an intermediate state of Li_xWO_3, leading to the color change from a transparent state to deep blue in color. After the applied electric field disappears, the Li^+ ions are trapped and the deep blue color can be maintained for some time, which is the so-called "color memory effect". When the reverse electric field is applied, the Li^+ ions could be de-trapped from the Li_xWO_3 films, and the WO_3 films return to their transparent state.

Notably, the colored pattern of the pixels in the electrochromic device was achieved easily by controlling the shape of the WO_3 film. As shown in Fig. S6 (ESI),† the ECD in the colored state realized a "NANO" pattern display by designing the shape of the WO_3 films. Under the reverse electric field stimulation, the device can be fully bleached. In our fabricated visible sensing and recording system, the pixel of the ECD array was designed as the square pattern (0.8×0.8 mm^2). Fig. S7a and b (ESI)† shows the schematic illustration of the structure of the ECD array and the equivalent circuit diagram. Under the stimulation of a positive electric field, all pixels can be colored and exhibit excellent uniformity (Fig. 3b and S7c, ESI†). Besides, there is no signal cross-talk among these pixels, which guarantees that all pixels can be colored independently. As demonstrated in Fig. S7d (ESI),† the pixels in the ECD array can be selectively colored by connecting the corresponding channels.

To quantificationally evaluate the electrochromic properties of the ECD, an ECD with a WO_3 film area of 1.5×1.5 cm^2 was fabricated (Fig. S8a, ESI†) and the device demonstrated obvious color changing at coloration and bleaching voltages of

3 V and −3 V, respectively (Fig. S8b, ESI†). Fig. 3c demonstrates the *in situ* transmittance (T) spectra from 300 to 800 nm of the corresponding device. The maximum optical modulation (ΔT_{max}) was observed at a wavelength of 633 nm, which is consistent with previously reported results.[48] Fig. 3d presents the switching test between coloration and bleaching of the as-fabricated ECD at the wavelength of 633 nm. The ΔT_{max} value of the device is as high as 27.5% and the coloration time and bleaching time are about 15 s and 2 s, respectively. As shown in Fig. S9 (ESI),† the color contrast of the ECD degraded about 9% after operating for 1.5 h, indicating that the device possesses a fine stability and reproducibility. The color retention capacity of the ECD was also characterized. Fig. 3e presents the process that the device was stimulated from the bleached state to the colored state, and further generated color memory without external voltage. It can be seen that the ΔT value retained 60% of ΔT_{max} after the external electric field disappears for 6 hours (Fig. 3f). The inset photographs present a gradual fading process of the colored device over time.

To further demonstrate the visible light sensing and recording functions, a customized experimental setup was built, as schematically illustrated in Fig. 4a. A mercury lamp that can generate parallel white light was employed as a light source. The designed mask was used to obtain an "H"-shaped light pattern. When the light was projected to the active area of the PD array, only those activated pixels were changed to the LRS state, resulting in the color change of the corresponding pixels in the ECD array. Subsequently, the displayed pattern was captured through a digital camera. In this work, the captured pattern was ultimately converted to a grayscale image by the programmed MATLAB software. As a prerequisite for the recording of the light pattern, the uniformity of the pixels in the system was firstly verified by illuminating all pixels of the PD array without using the designed mask (+3 V bias voltage). Fig. S10 (ESI)† shows the captured images and the corresponding grayscale images of all pixels in the bleached and colored states. Under the illumination with an intensity of 15 mW cm^{-2}, all pixels can be colored, which illustrates satisfactory uniformity of the system.

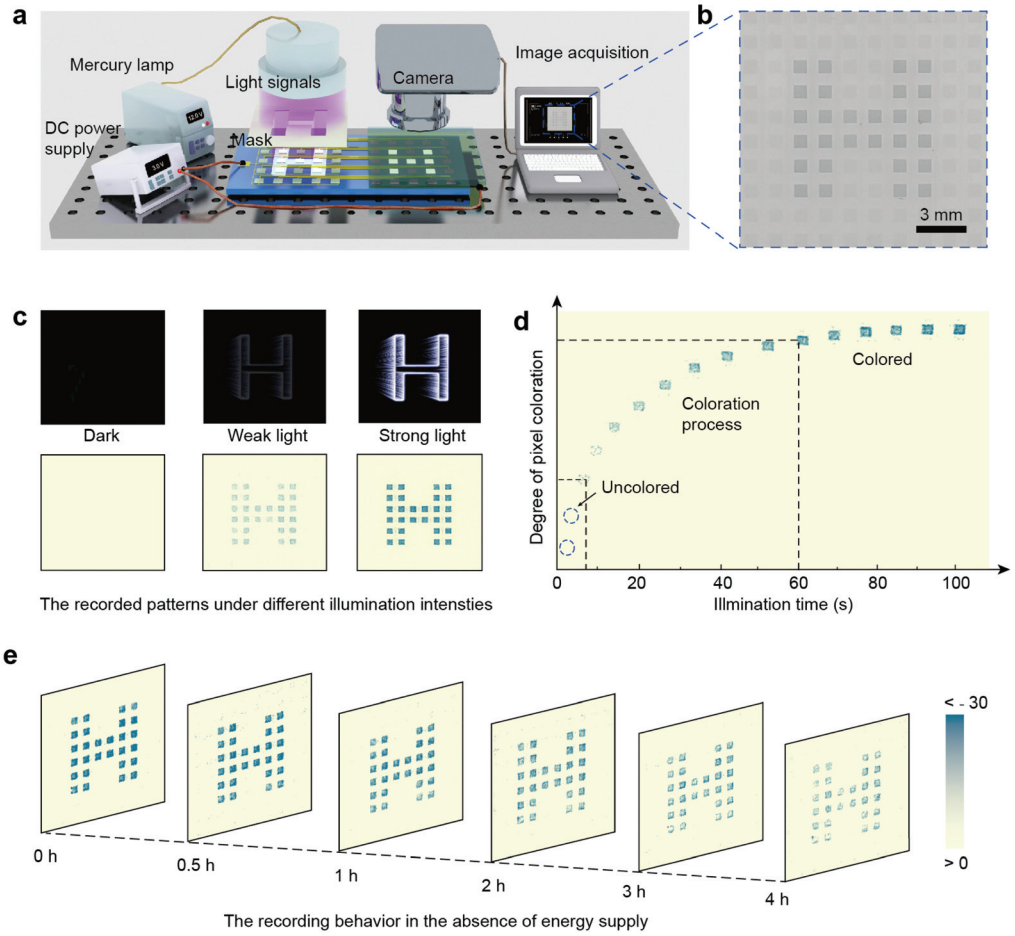

Fig. 4 The functional demonstration of visible light recording. (a) The schematic illustration of the experimental setups. (b) The optical photograph of the "H"-shaped pattern recorded by the system. (c) The recorded light patterns at different illumination intensities. (d) The acquired image of an activated pixel at each time point during the recording process at a light intensity of 15 mW cm^{-2}. (e) The grayscale image of the recorded "H"-shaped pattern after illumination stimulation for 100 s. After removing the illumination stimuli, the recording of the light pattern continues in the absence of the power supply.

The proof-of-concept of the recording of the visible light pattern was demonstrated by applying an "H"-shaped light stimulus on the PD array. As shown in Fig. 4b, a legible "H"-shaped colored pattern was displayed in the ECD array, illustrating the feasibility of the system for recording the light pattern. Fig. 4c presents the record light patterns after illuminating for 100 s at intensities of 0, 8, and 15 mW cm^{-2}, respectively. The recorded pattern became clearer as the light intensity increased, which is attributed to the large partial voltage applied on the ECD pixels at high illumination intensity that could drive a large amount of Li^+ ions to intercalate inside the WO_3 film. Besides, after removing the illumination stimuli, the recording of the light pattern continued in the absence of the power supply owing to the "color memory effect". When the applied electric field disappeared, the Li^+ ions in the triggered pixels were not allowed to rapidly de-intercalate due to ion trapping.[49] Thus, the triggered pixels can store the deep blue color for some time, while the untriggered pixels remain in the transparent state, achieving the recording of the light pattern in the absence of the power supply. The recorded time of the light pattern can be regulated through the periods of illumination stimulation. As illustrated in Fig. 4d, the colored intensity of the pixel gradually increased with the illumination time at a light intensity of 15 mW cm^{-2}. This was a process of Li^+ ion insertion and it also strengthened the memory. It was reported that Li^+ ions were trapped by "shallow sites" (with low-energy barriers) in a short coloration time.[50] Thus, these trapped Li^+ ions were allowed to be rapidly de-trapped from the WO_3 film after the electric field was removed, leading to rapid color fading. While applying a sufficiently long coloration time, the Li^+ ions can be trapped by "deep sites" (with high-energy barriers) that will recover slowly,[50] which facilitate long-term recording. As presented in Fig. S11 (ESI),† the recorded "H"-shaped pattern disappeared within 50 min after being illuminated for 40 s, while it could be recorded for more time once it was stimulated for 100 s. Fig. 4e shows the recorded "H"-shaped pattern after being illuminated for 100 s. The system can still retain the pattern shape with little attenuation after 4 hours, achieving long-time recording of the visible light pattern. The above survey verifies the optical information recording capability of the system.

Conclusions

In summary, we fabricated a visible light sensing and recording system by integrating the perovskite PD array and WO_3-based ECD device array. The PD array with satisfactory pixel uniformity exhibited excellent visible light sensing characteristics. The ECD exhibited 27.5% optical modulation at 3 V voltages and ΔT remained 60% of ΔT_{max} after the electric field disappeared for 6 hours, showing the capability of optical information recording. The investigation confirmed that the system can convert the received visible light signals into electrical signals to change the storable color of the corresponding pixels in the ECD array, thus realizing optical information recording in the form of the color display. The system achieves the recording of the "H"-shaped visible light pattern projected to the active area of the PD array. Besides, after removing the illumination stimuli, the recording of the light pattern continues in the absence of the power supply. The recorded length can be regulated through the periods of illumination stimulation. When the duration of the illumination stimuli was 100 s, the recorded light pattern could still be recognized with little attenuation after 4 hours. Such a visible light sensing and recording system can act as an intelligent robot to directly capture and store images in environments that are inaccessible to the human eyes. We predict that this system may have potential applications in image sensors, electronic eyes, and intelligent electronics.

Experimental section

Preparation of the patterned $CH_3NH_3PbI_{3-x}Cl_x$ perovskite film

0.8 M PbI_2 and 0.4 M $PbCl_2$ were dissolved in *N,N*-dimethylformamide (DMF) at 75 °C as precursor solution #1, and the CH_3NH_3I was dissolved in 2-propanol with a concentration of 40 mg mL^{-1} as precursor #2. The perovskite films were controllably synthesized by the previously reported two-step sequential deposition method.[40,41] Firstly, precursor solution #1 was spin-cast on the prepared substrate at 4000 rpm for 35 s. Next, precursor solution #2 was spin-coated onto $PbI_2/PbCl_2$ films at 4000 rpm for 35 s. Later, the extra CH_3NH_3I particles were cleaned using 2-propanol, and then an annealing process was conducted at 100 °C for 30 min to improve the crystallization.

Preparation of the polyelectrolyte

Firstly, anhydrous $LiClO_4$ was obtained by drying $LiClO_4{\cdot}3H_2O$ in a vacuum drying oven at 120 °C for 3 h. Next, anhydrous $LiClO_4$ was dissolved in propylene carbonate (1 M). Subsequently, poly(methylmethacrylate) (PMMA) was mixed into the prepared solution with a weight ratio of 25% and stirred at 100 °C for 5 h.

Fabrication of the visible light sensing and recording system

Firstly, a 2.5 cm × 5 cm glass with a thickness of 1 mm was ultrasonically cleaned and treated by oxygen plasma (O_2, 100 sccm, 200 W, 20 min) as a substrate. Second, the designed indium tin oxide (ITO) film (150 nm in thickness) electrode circuits were fabricated by the ultraviolet (UV) photolithography technique (MA6 SUSS) and radio frequency (RF) magnetron sputtering (Kurt J. Lesker PVD75). Third, a layer of the WO_3 film array (size 0.8 × 0.8 mm^2) was prepared. The dimensions and location of WO_3 films were defined by the UV photolithography technique and the film was deposited by RF magnetron sputtering under the conditions of $Ar:O_2$ = 30:20 sccm, sputtering power 120 W, and sputtering time 1 h. Fourth, for synthesizing the perovskite film array, the sample surface was treated to make the interdigital electrode region's surface hydrophilic and the other region's surface hydrophobic. Specifically, the oxygen plasma was employed again to

treat the whole surface for 60 s at a power of 50 W (O_2, 100 sccm). Next, the patterned photoresist mask (S1813) prepared by the UV photolithography technique was used to cover the interdigital electrodes and the whole ECD part, and a layer of the SiO_2 film was deposited. Then, the sample was soaked with a mixture of (octadecyl) trichlorosilane (OTS) and hexane (0.5% volume ratio). After 15 minutes, the sample was put into acetone to remove the photoresist mask. Fifth, the perovskite film was grown on interdigital electrodes by the two-step sequential deposition method. Finally, the polyelectrolyte was cast onto the WO_3 films and pressed together with a piece of ITO glass (2.5 cm × 3 cm) at a temperature of 100 °C.

Characterization studies and measurements

Field-emission scanning electron microscopy (SU8020, Hitachi) and X-ray diffraction (X'Pert3 Powder) were employed to conduct the morphological and phase analyses of the patterned $CH_3NH_3PbI_{3-x}Cl_x$ perovskite film. A UV-vis-NIR spectrophotometer (UV-3600, Shimadzu) was used to measure the absorption spectra of perovskite films and the transmittance of the ECD device. The electrical measurements of the device were performed using a Keithley 4200 SCS and an SR570 (Stanford Research Systems). The displayed images were captured using a digital camera. A mercury lamp (Lumen Dynamics XI120-Q) was used as the light source.

Author contributions

Wenqiang Wu, Xun Han, Caofeng Pan and Anlian Pan conceived and designed the project. Wenqiang Wu, Mengmeng Zhou, Xun Han, Zheng Yang and Zhihao Huo performed the device fabrication and property characterization studies. Wenqiang Wu, Xun Han, Shengman Li and Dong Li participated in experimental result discussions and paper writing. Yanqing Wu, Caofeng Pan and Anlian Pan supervised the experiments and provided theoretical guidance. All of the authors discussed and commented on the manuscript.

Conflicts of interest

The authors declare that they have no conflict of interest.

Acknowledgements

The authors acknowledge the support from the National Natural Science Foundation of China (No. U19A2090, 62090035, 51525202, 51772084, 51972105, 51622205, 61675027, and U20A20166), the Key Program of Science and Technology Department of Hunan Province (2019XK2001 and 2020XK2001), the National Key R & D project from the Minister of Science and Technology, China (2016YFA0202703), the Beijing City Committee of Science and Technology (Z171100002017019 and Z181100004418004), the Natural Science Foundation of Beijing Municipality (2184131, 4181004, 4182080, 4184110, and Z180011).

Notes and references

1 S. Cai, X. Xu, W. Yang, J. Chen and X. Fang, *Adv. Mater.*, 2019, **31**, e1808138.
2 X. Li, C. Gao, H. Duan, B. Lu, X. Pan and E. Xie, *Nano Energy*, 2012, **1**, 640–645.
3 X. Zhang, S. Yang, H. Zhou, J. Liang, H. Liu, H. Xia, X. Zhu, Y. Jiang, Q. Zhang, W. Hu, X. Zhuang, H. Liu, W. Hu, X. Wang and A. Pan, *Adv. Mater.*, 2017, **29**, 1604431.
4 X. Han, M. Chen, C. Pan and Z. L. Wang, *J. Mater. Chem. C*, 2016, **4**, 11341–11354.
5 C. Bao, J. Yang, S. Bai, W. Xu, Z. Yan, Q. Xu, J. Liu, W. Zhang and F. Gao, *Adv. Mater.*, 2018, **30**, e1803422.
6 C. Jiang and J. Song, *Adv. Mater.*, 2015, **27**, 4454–4460.
7 F. Xia, H. Wang, D. Xiao, M. Dubey and A. Ramasubramaniam, *Nat. Photonics*, 2014, **8**, 899–907.
8 K. Xia, W. Wu, M. Zhu, X. Shen, Z. Yin, H. Wang, S. Li, M. Zhang, H. Wang, H. Lu, A. Pan, C. Pan and Y. Zhang, *Sci. Bull.*, 2020, **65**, 343–349.
9 X. Yu, S. Zhang, H. Zeng and Q. J. Wang, *Nano Energy*, 2016, **25**, 34–41.
10 J. Fang, Z. Zhou, M. Xiao, Z. Lou, Z. Wei and G. Shen, *InfoMat*, 2019, **2**, 291–317.
11 F. Xia, T. Mueller, Y. M. Lin, A. Valdes-Garcia and P. Avouris, *Nat. Nanotechnol.*, 2009, **4**, 839–843.
12 L. Mennel, J. Symonowicz, S. Wachter, D. K. Polyushkin, A. J. Molina-Mendoza and T. Mueller, *Nature*, 2020, **579**, 62–66.
13 S. T. Ha, R. Su, J. Xing, Q. Zhang and Q. Xiong, *Chem. Sci.*, 2017, **8**, 2522–2536.
14 X. Han, W. Wu, H. Chen, D. Peng, L. Qiu, P. Yan and C. Pan, *Adv. Funct. Mater.*, 2020, **31**, 2005230.
15 F. Li, J. Lu, Q. Zhang, D. Peng, Z. Yang, Q. Xu, C. Pan, A. Pan, T. Li and R. Wang, *Sci. Bull.*, 2019, **64**, 698–704.
16 L. Zhang, Z. Luo, L. Su and D. Tang, *Analyst*, 2019, **144**, 5717–5723.
17 L. Su, P. Tong, L. Zhang, Z. Luo, C. Fu, D. Tang and Y. Zhang, *Analyst*, 2019, **144**, 4880–4886.
18 Y. Liu, Y. Zhang, K. Zhao, Z. Yang, J. Feng, X. Zhang, K. Wang, L. Meng, H. Ye, M. Liu and S. F. Liu, *Adv. Mater.*, 2018, **30**, e1707314.
19 L. Gu, S. Poddar, Y. Lin, Z. Long, D. Zhang, Q. Zhang, L. Shu, X. Qiu, M. Kam, A. Javey and Z. Fan, *Nature*, 2020, **581**, 278–282.
20 W. Wu, X. Han, J. Li, X. Wang, Y. Zhang, Z. Huo, Q. Chen, X. Sun, Z. Xu, Y. Tan, C. Pan and A. Pan, *Adv. Mater.*, 2021, **33**, e2006006.
21 H. P. Wang, S. Li, X. Liu, Z. Shi, X. Fang and J. H. He, *Adv. Mater.*, 2021, **33**, e2003309.

22 B. Yang, F. Zhang, J. Chen, S. Yang, X. Xia, T. Pullerits, W. Deng and K. Han, *Adv. Mater.*, 2017, **29**, 1703758.
23 Y. Dong, Y. Zou, J. Song, X. Song and H. Zeng, *J. Mater. Chem. C*, 2017, **5**, 11369–11394.
24 Z. Yang, Q. Xu, X. Wang, J. Lu, H. Wang, F. Li, L. Zhang, G. Hu and C. Pan, *Adv. Mater.*, 2018, **30**, e1802110.
25 J. Feng, C. Gong, H. Gao, W. Wen, Y. Gong, X. Jiang, B. Zhang, Y. Wu, Y. Wu, H. Fu, L. Jiang and X. Zhang, *Nat. Electron.*, 2018, **1**, 404–410.
26 L. Gu, M. M. Tavakoli, D. Zhang, Q. Zhang, A. Waleed, Y. Xiao, K. H. Tsui, Y. Lin, L. Liao, J. Wang and Z. Fan, *Adv. Mater.*, 2016, **28**, 9713–9721.
27 L. Shao, X. Zhuo and J. Wang, *Adv. Mater.*, 2018, **30**, e1704338.
28 W. Zhang, X. Wang, Y. Wang, G. Yang, C. Gu, W. Zheng, Y. M. Zhang, M. Li and S. X. Zhang, *Nat. Commun.*, 2019, **10**, 1559.
29 X. Cao, C. Lau, Y. Liu, F. Wu, H. Gui, Q. Liu, Y. Ma, H. Wan, M. R. Amer and C. Zhou, *ACS Nano*, 2016, **10**, 9816–9822.
30 Z. Yu, G. Cai, X. Liu and D. Tang, *Anal. Chem.*, 2021, **93**, 2916–2925.
31 Z. Yu, G. Cai, R. Ren and D. Tang, *Analyst*, 2018, **143**, 2992–2996.
32 X. Han, W. Du, M. Chen, X. Wang, X. Zhang, X. Li, J. Li, Z. Peng, C. Pan and Z. L. Wang, *Adv. Mater.*, 2017, **29**, 1701253.
33 H. Park, D. S. Kim, S. Y. Hong, C. Kim, J. Y. Yun, S. Y. Oh, S. W. Jin, Y. R. Jeong, G. T. Kim and J. S. Ha, *Nanoscale*, 2017, **9**, 7631–7640.
34 D. R. Rosseinsky and R. J. Mortimer, *Adv. Mater.*, 2001, **13**, 783–793.
35 E. J. Yoo, M. Lyu, J. H. Yun, C. J. Kang, Y. J. Choi and L. Wang, *Adv. Mater.*, 2015, **27**, 6170–6175.
36 F. Zhou, Y. Liu, X. Shen, M. Wang, F. Yuan and Y. Chai, *Adv. Funct. Mater.*, 2018, **28**, 1800080.
37 R. Dong, Y. Fang, J. Chae, J. Dai, Z. Xiao, Q. Dong, Y. Yuan, A. Centrone, X. C. Zeng and J. Huang, *Adv. Mater.*, 2015, **27**, 1912–1918.
38 W. Deng, L. Huang, X. Xu, X. Zhang, X. Jin, S. T. Lee and J. Jie, *Nano Lett.*, 2017, **17**, 2482–2489.
39 W. Tian, H. Zhou and L. Li, *Small*, 2017, **13**, 1702107.
40 W. Wu, X. Wang, X. Han, Z. Yang, G. Gao, Y. Zhang, J. Hu, Y. Tan, A. Pan and C. Pan, *Adv. Mater.*, 2019, **31**, e1805913.
41 Y. Lin, G. Lin, B. Sun and X. Guo, *Adv. Funct. Mater.*, 2018, **28**, 1705589.
42 M. M. Lee, J. Teuscher, T. Miyasaka, T. N. Murakami and H. J. Snaith, *Science*, 2012, **338**, 643–647.
43 N. Dong, X. Fu, G. Lian, S. Lv, Q. Wang, D. Cui and C. P. Wong, *ACS Appl. Mater. Interfaces*, 2018, **10**, 8393–8398.
44 A. Subrahmanyam and A. Karuppasamy, *Sol. Energy Mater. Sol. Cells*, 2007, **91**, 266–274.
45 J. Li, X.-Y. Zhang, Y.-B. Liu, Y.-G. Li and R.-P. Liu, *Rare Met.*, 2013, **32**, 512–517.
46 Q.-S. Zhou, Y.-K. Chen, X.-B. Li, T.-G. Qi, Z.-H. Peng and G.-H. Liu, *Rare Met.*, 2017, **37**, 604–612.
47 H.-H. Lu, *J. Alloys Compd.*, 2008, **465**, 429–435.
48 D. Ma, G. Shi, H. Wang, Q. Zhang and Y. Li, *J. Mater. Chem. A*, 2013, **1**, 684–691.
49 F. Fabregat-Santiago, G. Garcia-Belmonte, J. Bisquert, N. S. Ferriols, P. R. Bueno, E. Longo, J. S. Anton and S. Castro-Garcia, *J. Electrochem. Soc.*, 2001, **148**, E302–E309.
50 R. T. Wen, C. G. Granqvist and G. A. Niklasson, *Nat. Mater.*, 2015, **14**, 996–1001.

